Emergent Chemical Mapping at Atomic-Column Resolution by Energy-Dispersive X-Ray Spectroscopy in an Aberration-Corrected Electron Microscope

M.-W. Chu,[1] S. C. Liou,[1] C.-P. Chang,[1,2] F.-S. Choa,[3] and C. H. Chen[1,4,*]

[1]*Center for Condensed Matter Sciences, National Taiwan University, Taipei 106, Taiwan*
[2]*Department of Material Sciences and Engineering, National Taiwan University, Taipei 106, Taiwan*
[3]*Department of Computer Science and Electrical Engineering, University of Maryland, Baltimore County, Maryland 21250, USA*
[4]*Department of Physics, National Taiwan University, and Institute of Atomic and Molecular Sciences, Academia Sinica, Taipei 106, Taiwan*

(Received 1 February 2010; published 11 May 2010)

Chemical mapping at atomic-column resolution by energy-dispersive x-ray spectroscopy in a spherical aberration-corrected scanning transmission electron microscope (STEM) has been demonstrated for the 1.47-Å dumbbell structure in InGaAs. The structural imaging and the chemical information in the two-dimensional map are directly correlated. Comparisons with the other existing mapping techniques of STEM in conjunction with electron energy-loss spectroscopy were discussed from aspects of ionization interactions.

DOI: 10.1103/PhysRevLett.104.196101 PACS numbers: 68.37.Lp, 73.20.Jc, 73.21.Cd, 78.70.En

Unraveling the correlations between structural details and physical properties continues to be an outstanding problem in material research [1,2]. An understanding of the chemical information at atomic-column resolution holds fundamental importance toward this goal and poses great challenges for scientists to identify an atomic column both spatially and spectroscopically [1–5].

With the incorporation of a spherical aberration (C_s) corrector into a scanning transmission electron microscope (STEM), a one-angstrom-scale electron probe now becomes routine and one can resolve atomic columns with atomic-number (Z) contrasts through high-angle annular dark-field (HAADF) imaging of predominantly phonon scattered electrons (thermal diffused scattering, TDS) beyond Bragg diffraction angles [4–7]. Meanwhile, the C_s correction greatly increases the STEM probe current, enhancing the spectral signal-to-noise ratio and thus opening up vast opportunities for analytical works at atomic-column resolution [4–7]. Indeed, chemical mapping at atomic-column resolution by C_s-corrected STEM was demonstrated in combination with electron energy-loss spectroscopy (EELS; thus STEM-EELS) that characterizes the chemical information of atomic species by inelastic core level excitations [4,5,8,9]. However, the chemical mapping by STEM-EELS, under some circumstances, could be nonintuitive such as the observed chemical contrast reversal as a function of loss energies for a given EELS edge taken at given atomic columns and the intermixing of EELS signals from neighboring and chemically distinct atomic columns [9–13], despite unambiguous mapping having been otherwise reported [4,5].

Here, we report the experimental demonstration of another chemical mapping at atomic-column resolution using STEM in conjunction with energy-dispersive x-ray spectroscopy (EDX; thus STEM-EDX), which collects characteristic x rays as a function of probe positions instead of inelastic scattered electrons acquired in STEM-EELS. The direct linkage between the atomic column and the chemical information in our STEM-EDX mapping is discussed in the context of the ionization interaction understood for both STEM-EDX and STEM-EELS, which takes into consideration the dynamical electron channeling in specimens and the effective ionization potential of inelastic events [9–12,14,15]. This STEM-EDX mapping technique was unexpected due to the common notion of EDX as a tool for bulk chemical characterizations [16]. Comparisons with underlying principles for the established STEM-EELS mapping are also addressed.

We investigated $In_{0.53}Ga_{0.47}As$ and $In_{0.52}Al_{0.48}As$ superlattices in this work, abbreviated as InGaAs and InAlAs, respectively. The superlattices were grown on n-type InP substrate and the growth details were published elsewhere [17,18]. The specimen was prepared by wedge polishing, followed by short low-energy ion milling at 0.3 keV to remove the amorphous overlayers [4]. Our STEM is a field-emission JEOL-2100F microscope, operated at 200 keV and equipped with a probe C_s corrector of CEOS GmbH. The HAADF collection inner and outer radii are of 70 and 187 mrad, respectively. The EDX spectrometer is a Bruker XFlash-5030, liquid-nitrogen-free silicon drift detector with an optimized collection solid angle of ~0.13 steradian. STEM calculations were performed using the multislice method [19].

Figure 1(a) shows a [110] cross-sectional HAADF image of the InGaAs/InAlAs superlattices, acquired with a probe size ~1 Å (probe convergent semiangle, 20 mrad) and a probe current ~33 pA and subsequently subjected to image background removals using the method previously suggested in Ref. [20]. This probe condition was exploited throughout our experiments and the characteristic dumbbell structure of the materials along the [110] projection was nicely resolved [Fig. 1(a)]. The thickness estimation of

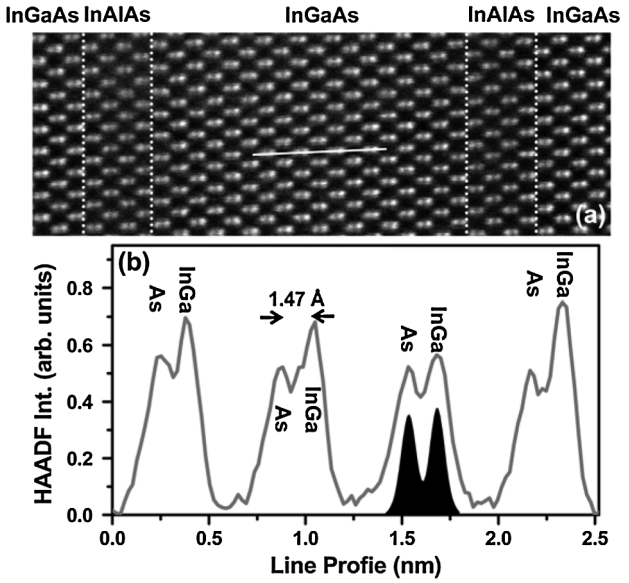

FIG. 1. (a) The [110] cross-sectional HAADF image of the InGaAs/InAlAs superlattices with background-removed using the method indicated in Ref. [20]. (b) The HAADF-intensity line profile of the solid white line (10 pixels in width, not shown for simplicity) in (a), revealing the dumbbell atomic columns of InGaAs with a spacing of 1.47 Å and the intensity variations due to local chemical inhomogeneities. The black filled curve represents the calculated HAADF intensity profile for an InGaAs dumbbell with nominal stoichiometry (see text for details).

this sample region by the method of EELS Fourier log-ratio yielded a value of ~29 nm. A close examination of the dumbbell atomic-column spacing by the line profile indicated in Fig. 1(a) (solid white line) reaffirms a homogeneous column spacing of 1.47 Å for the dumbbells [Fig. 1(b)]. Hereinafter, we focus on InGaAs only, since InAlAs layers are more susceptible to radiation damage during the slow scans necessary for sufficient STEM-EDX spectral counts, whereas InGaAs layers are more resistant.

On the basis of the relatively uniform baseline [Fig. 1(b)] characteristic to background-removed HAADF images [20], we observed variations in the atomic-column Z contrasts, which are the HAADF intensity ratios of (InGa)/As columns, suggesting a local chemical inhomogeneity [19,20]. In Fig. 1(b), the black filled curve under the specific (InGa), As column indicates the calculated HAADF intensity profile using the nominal composition, the experimental probe and HAADF conditions, the TDS-related Debye-Waller (DW) factors of GaAs (Ga, 0.637 Å^2; As, 0.685 Å^2) [19,21], and the sample thickness of 29.4 nm (50 cells; cell, $a = 5.88$ Å). These DW factors are good compromises in our cases, though not exact, since slight modifications do not noticeably change the thus-calculated Z contrast.

The calculated Z contrast of 1.06 in Fig. 1(b) is close to the experimentally determined value of 1.08 for the (InGa), As column on top of the calculated profile, suggesting the relative stoichiometry of this column compared to the nominal composition. The larger Z contrasts in the other (InGa), As columns in Fig. 1(b) then evidence the chemical inhomogeneities. Local chemical inhomogeneities with various Z contrasts were also observed in the other InGaAs columns in Fig. 1(a) and the other InGaAs regions in the sample with a similar thickness of ~29 nm. Having established the local inhomogeneities by HAADF, we now turn to the chemical mapping by STEM-EDX.

Using the aforementioned electron-optics calculation conditions, we show in Figs. 2(a)–2(c) the $[1\bar{1}0]$-projected intensities of the [110]-incident electron wave function with the electron probe focused on an InGa column (a), an As column (b), and an open site in InGaAs (c) and propagating through a thickness of 50 unit cells (~29 nm). The dynamical, elastic scattering of fast electrons in crystalline materials gives rise to the characteristic dynamical channeling along InGa and As columns in Figs. 2(a) and 2(b), respectively, [particularly, Fig. 2(b)] [9–13,22]. For a thickness above ~40 cells (~23.5 nm) in Fig. 2(a), a portion of the intensity of the incident wave function has spread out to the neighborhood, known as the electron dechanneling due to an effect of significant TDS mediated by heavy elements and/or elements with large DW factors [9–13,22]. The heavy In element in the InGa column accounts for this dechanneling in the thick specimen limit [Fig. 2(a)], since Ga and As are similarly weighted with comparable DW factors [19,21]. In Fig. 2(c), the electron dechanneling along an open site is drastic despite the forward scattering character of such a high-energy electron probe. This notable dechanneling is correlated with the vanishing elastic potential therein [Fig. 2(d)] to guide the incident electrons and should be ultimately minimized for spectral mapping with very thin specimens [9,10]. Positioning the electron probe over an open site in a thick sample [e.g., above ~10 nm, Fig. 2(c)], it still sees InGa and As columns due to beam broadening, i.e., the spectral cross talk effect reported previously [9,10].

Figure 3(a) shows the STEM-EDX mapping of an InGaAs region (thickness, ~29 nm), 16×34 pixels, 3 ms of dwell time per pixel, and 13 s of total mapping time plus readouts. Chemical mapping demonstrating the structural dumbbell at atomic-column resolution was unambiguously achieved with direct correlations to the spatial imaging [corresponding HAADF inset, Fig. 3(b)]. Figure 3(b) shows the corresponding integrated EDX spectrum and the spectral ranges used for the mapping [In (blue), Ga (green), and As (orange)] [23]. The minor residual contrasts between the given columns in each of the individual chemical maps [In, Ga, and As; Fig. 3(a)] are correlated with the spectral cross talk due to electron dechanneling [9,10], which consequently represents a limiting factor in our current mapping. For the In map [top-left panel, Fig. 3(a)], the missing In chemical contrast in the right-bottom InGa column [replenished by the Ga chemical contrast; bottom-left panel, Fig. 3(a)] should

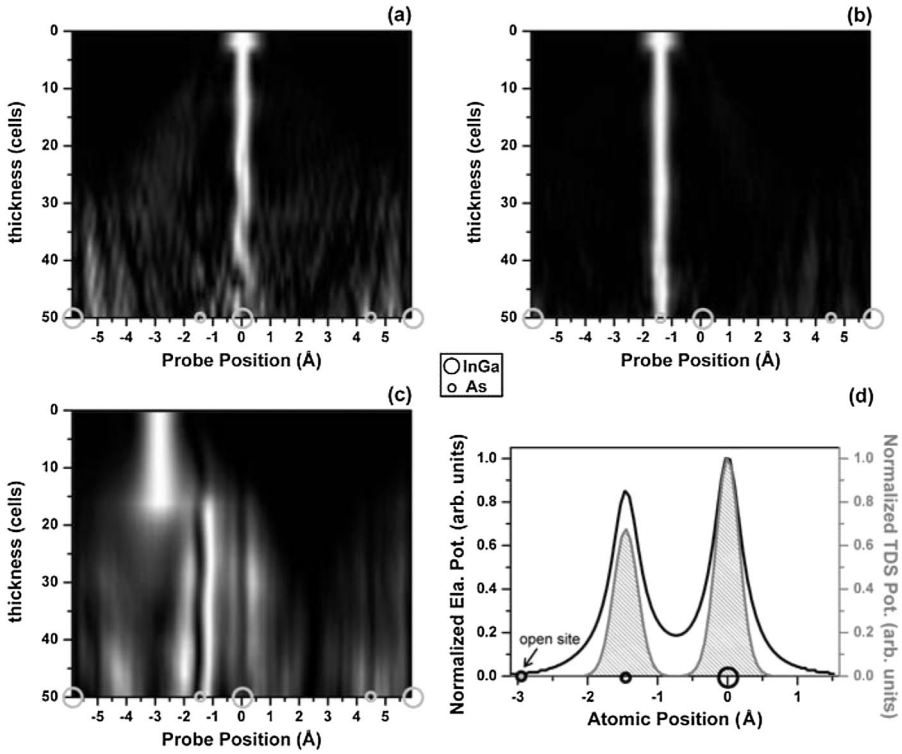

FIG. 2. The $[1\bar{1}0]$-projected intensities of the [110]-incident electron wave function in InGaAs with the electron probe focused on an InGa column (a), an As column (b), and an open site in InGaAs (c) and propagating through a thickness of 50 unit cells (~29 nm). The gray level is in linearly normalized scale, black for 0 and white for 1. (d) The elastic (black) and TDS (gray) potentials are characteristic to the STEM calculations in (a)–(c) with the potentials normalized to the respective maxima on the InGa column.

rather be related to the local chemical inhomogeneities indicated in Fig. 1, because the derived Z contrast of this column, ~0.99, though noisy [inset, Fig. 3(b)], is close to 0.98 calculated for Ga/As using GaAs of ~29 nm in thickness. The spectral statistics in Fig. 3(b) are, however, insufficient for statistically meaningful chemical quantifications let alone column-specific quantifications using weaker pixel-based spectra. Further explorations of the quantitative limit for this emergent STEM-EDX mapping such as the established single-atom sensitivity in STEM-EELS [8] can be the next exciting challenge.

The two-dimensional chemical mapping with a direct correspondence between the structural imaging and the chemical information, Fig. 3(a), results from the electron channeling (Fig. 2) and the minimization of the associated spectral cross talk. The possible spurious x-ray signals due to scatterings of strayed incident electrons and high-energy secondary or backscattered electrons are estimated to not be significant enough to affect our STEM-EDX mapping at atomic-column resolution [Fig. 3(a)] using a thin specimen of ~29 nm [16]. Our achievement in Fig. 3 then properly depicts the picture that fulfills the *local* ionization interaction understood for two-dimensional chemical mapping using a fine electron probe, i.e., the mapping being the direct convolution of the channeling electron wave function and the effective *local* ionization potential [10,13]. To get a quantitative description of the effective local ionization potential related to the x-ray emissions in Fig. 3(b), the local character of a TDS potential with a half width at half maximum (HWHM) of $\sim 0.2/\sim 0.2$ Å for InGa/As columns was shown in Fig. 2(d) [14,19]. Although an exact calculation of the current effective local ionization potential is beyond our scope due to the subtle first-principles details [14,15], Fig. 2(d) (TDS potential) can capture the local electronic essence considering that its Gaussian line shape is close to the reported local Ga/As x-ray K-line ionization potential in GaAs with HWHM of 0.118/0.121 Å along the dumbbell direction [15].

For STEM-EELS, inelastic scattered electrons in the forward scattering direction are collected within an angular range [3–5,9,10]. Using a STEM-EELS collection semiangle (β) smaller than the probe convergent semiangle (α), one effectively samples the inelastic scattering and the elastic diffraction contrasts in a coherent imaging condition [10,12,13,24], giving rise to an effective nonlocal ionization potential [10]. In fact, a related intermixing of EELS signals from nearby, distinct atomic columns has been reported [10].

Applying the incoherent imaging condition of $\beta > \alpha$ for STEM-EELS, on the other hand, leads to an otherwise effective local ionization potential and the dynamical electron channeling becomes a predominant factor in the spatial resolving power of the chemical mapping [9,10,12,13], similar to our case of STEM-EDX. For STEM-EDX, one in effect collects x rays emitted from the sample over a solid angle of ~0.13 steradian that integrates essential kinetics of the inelastic electron scattering associated with the radiations (i.e., inelastic electron scattering over the whole momentum space followed by filling the core hole with a subsequent x-ray emission) [10,14,15], thus comparable to incoherent STEM-EELS spectral imaging with $\beta > \alpha$ [10]. Theoretical works on STEM-EDX indeed revealed

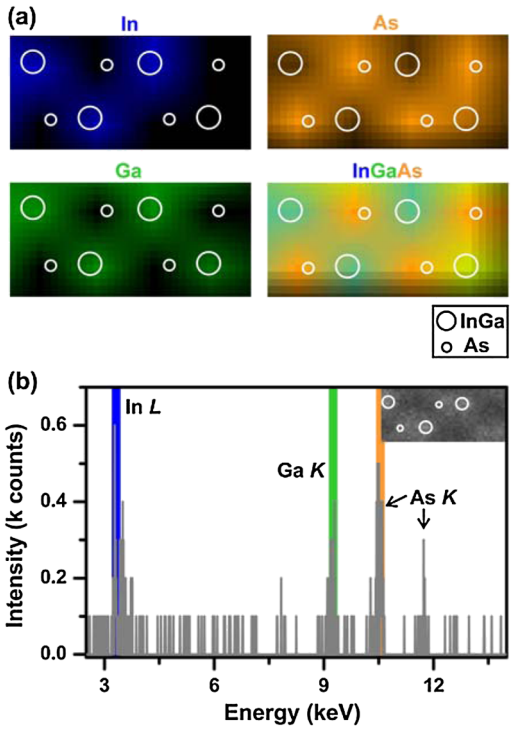

FIG. 3 (color online). (a) The STEM-EDX chemical mapping results for In, Ga, As, and the overlay of them. Open white circles, the atomic-column positions derived from the corresponding HAADF structural imaging in the inset of (b). Note that the missing In chemical contrast in the right-bottom InGa column is replenished by the Ga chemical contrast in the bottom-left panel. (b) The integrated EDX spectrum and the associated spectral ranges exploited for the mapping in (a). Details of mapping are given in Ref. [23].

an effective local ionization potential and proposed a local ionization interaction, i.e., the straightforward correlations between structural, chemical information in the two-dimensional chemical mapping [10].

In summary, we have experimentally demonstrated the STEM-EDX chemical mapping for the 1.47-Å dumbbell structure of InGaAs. An apparent advantage of STEM-EDX over STEM-EELS in the incoherent imaging regime is the efficiency of EDX detections of deep inner-shell ionizations above 2 keV [Fig. 3(b)], marginal for EELS. Inelastic scattering collected in EELS is prone to electronic delocalization with a length scale inversely proportional to the ionization energy [3,9–15,24]. Straightforward structural, chemical correlations in STEM-EELS incoherent imaging thus often require the utilization of deeper ionizations [3], of which the EELS detection becomes increasingly difficult. Otherwise, ambiguous results could still arise, such as the chemical contrast reversals in incoherent imaging for the shallow Si EELS L edge in thick specimens [9]. Alternatively, STEM-EDX stands for an emergent, complementary chemical mapping at atomic-column resolution with an unambiguous linkage between the structure and its chemical information using the efficient collection of x-ray emissions from deep ionizations.

The authors thank Professor L. J. Allen for helpful comments on the experimental results and Dr. K. Ishizuka for fruitful discussion on the channeling simulations. This work was supported by the National Science Council of Taiwan (NSC98-2628-M-002-009, NSC96-2112-M-002-031-MY3, and NSC98-2120-M-002-011) and the National Taiwan University Excellence Project No. (NTU98R0066-19).

Note added in proof.—We became aware of a very recent work [25], which also reports on STEM-EDX mapping at atomic-column resolution.

*Corresponding author; chchen35@ntu.edu.tw

[1] J. P. Buban *et al.*, Science **311**, 212 (2006).
[2] A. Ohtomo *et al.*, Nature (London) **419**, 378 (2002).
[3] K. Kimoto *et al.*, Nature (London) **450**, 702 (2007).
[4] D. A. Muller *et al.*, Science **319**, 1073 (2008).
[5] M. Bosman *et al.*, Phys. Rev. Lett. **99**, 086102 (2007).
[6] M. Haider *et al.*, Ultramicroscopy **81**, 163 (2000).
[7] O. L. Krivanek *et al.*, Ultramicroscopy **108**, 179 (2008).
[8] M. Varela *et al.*, Phys. Rev. Lett. **92**, 095502 (2004).
[9] P. Wang *et al.*, Phys. Rev. Lett. **101**, 236102 (2008).
[10] M. P. Oxley *et al.*, Phys. Rev. Lett. **94**, 203906 (2005).
[11] L. J. Allen, Phys. Rev. Lett. **91**, 105503 (2003).
[12] M. P. Oxley *et al.*, Phys. Rev. B **76**, 064303 (2007).
[13] K. Kimoto *et al.*, Micron **39**, 257 (2008).
[14] L. J. Allen and C. J. Rossouw, Phys. Rev. B **47**, 2446 (1993).
[15] M. P. Oxley and L. J. Allen, Phys. Rev. B **57**, 3273 (1998).
[16] D. B. Williams and C. B. Carter, *Transmission Electron Microscopy* (Plenum Press, New York, 1996).
[17] J. Yan *et al.*, IEEE Photonics Technol. Lett. **18**, 1777 (2006).
[18] X. J. Wang *et al.*, Appl. Phys. Lett. **90**, 211103 (2007).
[19] K. Ishizuka, Ultramicroscopy **90**, 71 (2002).
[20] P. D. Robb and A. J. Craven, Ultramicroscopy **109**, 61 (2008).
[21] J. S. Reid, Acta Crystallogr. Sect. A **39**, 1 (1983).
[22] J. M. LeBeau *et al.*, Phys. Rev. B **79**, 214110 (2009).
[23] To reduce the noise, the respective Ga (9.25 keV), As (10.55 keV), and In (3.29 keV) spectral signals acquired at each pixel in Fig. 3(a) were first Gaussian fitted by an automatic software function written in the Bruker spectrometer program. A mask of 87% of the area under each element was then used to pick up the spectral intensity needed for constructing each chemical map.
[24] D. A. Muller and J. Silcox, Ultramicroscopy **59**, 195 (1995).
[25] A. J. D'Alfonso *et al.*, Phys. Rev. B **81**, 100101(R) (2010).